J. Fluid Mech. (1990), *vol.* 221, *pp.* 23–52
Printed in Great Britain

Evolution of weakly nonlinear waves in a cylinder with a movable piston

By MENG WANG AND D. R. KASSOY
Department of Mechanical Engineering, University of Colorado, Boulder, CO 80309-0427, USA

(Received 12 April 1989 and in revised form 2 April 1990)

Small-amplitude wave motion in an inert gas confined between a moving piston and a fixed cylinder endwall is studied using the unsteady Euler equations. The waves, generated by either initial disturbances or piston motion, reflect back and forth in the cylinder on the acoustic timescale. The accumulated effect of these waves controls the bulk variations of velocity and thermodynamic variables on the longer piston timescale. Perturbation methods, based on the small ratio of acoustic to piston time, are employed to formulate the gasdynamic problem. The application of multiple timescaling allows the gasdynamic wave field to be separated from the bulk response of the gas. The evolution of the wave phenomena, including nonlinear wave deformation and weak shock formation during the piston passage time, is described in terms of time-dependent Fourier series solutions, whose coefficients are computed from a truncated system of coupled nonlinear ordinary differential equations. The long-time asymptotic flow field after shock formation is sawtooth-like, in which case the Fourier modes become decoupled. A remarkably simple relation between the shock amplitude and piston velocity is discovered. It is demonstrated that (i) the wave amplitude and frequency strongly depend on the piston motion; (ii) shock waves can be damped in a significant way by internal dissipation; and (iii) the mathematical approach developed in this study possesses certain advantages over the more traditional method of characteristics.

1. Introduction

This paper describes a theoretical investigation of piston-generated gasdynamic compression and expansion processes. Small-amplitude wave motion is studied in a gas-filled cylinder, shown in figure 1, which is closed at each end by a moving piston and a fixed cylinder wall respectively. The confined gas is assumed ideal and inert, with an initial mean state given by (p_0^*, ρ_0^*, T_0^*). The piston traverses the cylinder length L^* with an arbitrarily prescribed time-dependent velocity U_p^*. In the meantime gasdynamic waves, generated by either initial disturbances or piston motion, propagate back and forth across the cylinder with an acoustic speed large compared to U_p^*. The purpose of the present work is twofold: (i) to develop a basic understanding of the gasdynamic effects occurring in the system; and (ii) to explore efficient mathematical tools that can describe wave motion in a confined, variable-volume gas medium.

The study of wave motion inside a cylinder is motivated by potential applications to engine-related research. It has been recognized that traditional equilibrium thermodynamics cannot accurately describe the compression and expansion processes in an internal combustion engine. The gasdynamic disturbances that are

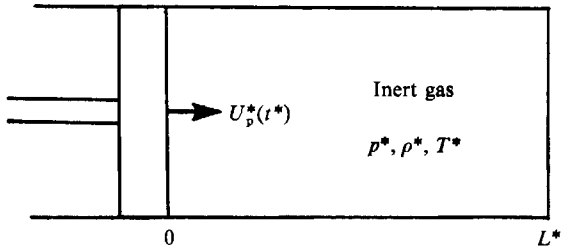

FIGURE 1. The physical system: an ideal inert gas in a cylinder confined by a moving piston.

excluded in equilibrium calculations are inevitably generated by various physical and/or chemical sources. The repeated passage of the gasdynamic waves across the cylinder is associated with non-uniform spatial distributions of pressure, density, temperature and velocity of the cylinder gas. These non-uniformities, albeit small in magnitude, can significantly affect self-ignition and combustion processes in a cylinder (Klein & Peters 1988). In this respect, a preliminary study of an inert gasdynamic system based on non-equilibrium formulations can be of practical as well as basic scientific interest.

Small-amplitude gasdynamic waves are frequently studied by using perturbation techniques in combination with the analytical method of characteristics (see, for example, Lighthill 1949; Lin 1954; Betchov 1958; Kluwick 1981). Schneider (1981) first applied this method to the piston–cylinder problem with extensive piston motion. In his study the multiple reflections of a weak shock wave generated by an initial impulsive piston motion are considered. A multiple-timescale analysis is used to resolve the many shock reflections that occur during the relatively long period of piston motion. The results are used to explain how multiple passage of a weak shock through a cylinder causes the observed bulk compression process. In order to construct the equations for characteristic lines and the compatibility relations along these lines, both dependent variables and independent space and time variables are expanded asymptotically based on small piston Mach number. However, Schneider was unable to obtain uniformly valid solutions for coordinate perturbations. Later, Klein & Peters (1988) realized that the non-uniformity in Schneider's asymptotic solutions was caused by the variation in wave passage time across the cylinder, as a result of piston-generated compression. A progressively stretched time variable was applied to adjust such changes. Uniformly valid solutions for gasdynamic quantities as well as characteristic coordinates were obtained. Their results show explicitly the shock formation processes from initially smooth compression waves, based on the development of multivalued regions in the characteristic space. A theory is developed to predict the shock formation time in terms of the initial wave shape and the piston motion. The analysis is extended further to chemically reactive systems to investigate the cumulative effects of the wave passages on the self-ignition of an explosive mixture.

The characteristic-coordinate perturbation technique is effective for solving the piston–cylinder problem, but exhibits several limitations. For example, the number of equations describing the physical system is increased owing to the coordinate transformations. In the asymptotic procedure the time and space variables must also be expanded asymptotically, in addition to the unknown dependent variables. More importantly, the secular equations for the first-order solutions, as developed by Klein & Peters (1988), are first-order partial differential equations. A rather sophisticated numerical scheme capable of resolving discontinuities must be

employed, and solutions can be obtained only at discrete values of time and space. In addition, it is difficult to interpret the mathematical results in order to find the explicit effect of the acoustic waves on the development of the bulk motion and properties.

An alternative mathematical tool, the Fourier series method, has also been applied to the study of acoustic wave motion in confined regions. For example, Kassoy (1979) and Radhwan & Kassoy (1984) employed this technique in combination with the multiple timescaling to describe linear acoustic waves generated in a gas-filled slot by boundary heating. In Ochmann's (1985) Fourier-series-based study of nonlinear resonant oscillations in a closed tube, the averaging method, which is closely related to the multiple-timescale technique, is used to describe the slowly changing wave amplitude. Transport effects are retained in his analysis so that mathematical difficulties associated with discontinuities are eliminated. The oscillation is driven by a distributed external forcing term. Ochmann derived an infinite system of coupled nonlinear ordinary differential equations for the Fourier coefficients. The Fourier system is summable when transformed into characteristic coordinates, and leads to an inhomogeneous Burgers equation. The above studies are restricted to constant-volume systems, so that no changes in the average gas state are included.

Wang & Kassoy (1990*a*) applied the Fourier series technique to consider the acoustic wave field generated by fast piston acceleration on the short acoustic timescale of the cylinder, and its subsequent development during the much longer time period when the piston travels towards the cylinder wall with constant speed. A multiple-timescale formulation was applied to separate the bulk compression of the gas from the instantaneous acoustic wave field. The latter was represented as infinite summations of spatially decomposed Fourier modes. In the nonlinear regime the Fourier coefficients are functions of the piston time, governed by an infinite system of equations similar to those found by Ochmann (1985). They were evaluated numerically to the desired truncation level. This straightforward method is shown to be capable of describing nonlinear wave deformation and weak shock formation processes during the piston time compression. The analysis is, however, rather restrictive in the sense that it describes only a single-stroke compression by a basically constant-speed piston.

In the present study we develop a Fourier-series-based solution for more general piston-driven gasdynamic motion inside the cylinder, shown in figure 1. The piston velocity is described by an arbitrary function of piston time. The initial state of the gas is specified in terms of disturbance velocity and density distributions in the cylinder, which simulate small-amplitude waves generated previously by various physical and chemical sources. It is the objective of the present work to study the influence of the varying background state of the gas on the development of the wave field, including wave deformation and possible shock formation, and to show the accumulative effect of small-amplitude waves on the global compression and expansion of the gas. The analytical approach employed in the present investigation is basically the same as that used in our previous study (Wang & Kassoy 1990*a*). Calculations are carried out for a variety of initial disturbances, when the piston moves forward, backward or cyclically. In particular, the standing sawtooth wave, which represents the long-time asymptotic flow field due to the shock generated in the cylinder, is examined in detail. In this case the Fourier mode coupling vanishes, and a simple solution is obtained to relate the shock amplitude to the subsequent smoothly varying piston motion. The present study demonstrates the versatility of the Fourier series technique in dealing with wave propagation processes. A

comparison is made between our approach and the more conventionally employed characteristics method.

2. Formulation

First, several important timescales of the closed piston–cylinder system shown in figure 1 must be introduced to provide readers with clearer physical insight into the formulation which follows. The characteristic time for acoustic wave transmission is defined as the acoustic timescale:

$$t_a^* = \frac{L^*}{c_0^*}, \tag{1}$$

where $c_0^* = (\gamma R^* T_0^*)^{\frac{1}{2}}$ is the sound speed based on the initial reference state of the gas. Another important time in the system is the piston timescale,

$$t_p^* = \frac{L^*}{U_{p_{ch}}^*}, \tag{2}$$

which represents time required for the piston to complete one stroke. $U_{p_{ch}}^*$ in (2) is the characteristic velocity of the piston. Note that the ratio of the acoustic time to piston time is the characteristic piston Mach number defined as the ratio of the characteristic piston speed to the speed of the sound c_0^*,

$$\epsilon \equiv \frac{U_{p_{ch}}^*}{c_0^*} = \frac{t_a^*}{t_p^*}. \tag{3}$$

Since initial disturbances are allowed to exist in the cylinder, the characteristic gas velocity U_g^* can be different from $U_{p_{ch}}^*$. Therefore it is necessary to define

$$t_g^* = \frac{L^*}{U_g^*} \tag{4}$$

as the characteristic time of gas motion. If the velocity field in the gas is exclusively caused by piston motion, the gas has the same characteristic time as that of the piston. The longest time used in the analysis is the conduction time defined as

$$t_c^* = \frac{L^{*2}}{\kappa_0^*}, \tag{5}$$

where κ_0^* is the thermal diffusivity of the initial reference state. For typical gases like air at normal conditions, where the Prandtl number is of $O(1)$, (5) defines the timescale required for both thermal and momentum diffusion to affect the gasdynamic process in a significant way (Radhwan & Kassoy 1984).

The order of magnitude of the quantities mentioned above can be calculated by considering a typical automobile engine with a shaft rotation of 3000 r.p.m. and a piston stroke of 0.08 m. One finds in this engine a maximum piston Mach number $\epsilon \approx 3.7 \times 10^{-2}$, a piston travelling time of $t_p^* \approx 10^{-2}$ s, and an acoustic wave travelling time of $t_a^* \approx 2.4 \times 10^{-4}$ s based on a sound speed of $c_0^* = 340$ m/s. The conduction time calculated under ambient conditions ($T_0^* = 300$ K, $p_0^* = 1$ atm) is $t_c^* \approx 290$ s. The velocity disturbance in a real engine cylinder may be caused by fast heat release

resulting from turbulent flame propagation during the combustion process, or by gas exchange during the intake or exhaust phases. It is normally small with respect to the sound speed. According to Klein & Peters (1988) the typical gas exchange velocity is about 30 m/s, thus $t_g^* = L^*/U_g^* \approx 2.7 \times 10^{-3}$ s.

The above data suggest that the analysis can be carried out under the following reasonable conditions:

$$\frac{t_g^*}{t_p^*} = O(1); \quad \frac{t_a^*}{t_p^*} = \epsilon \ll O(1); \quad \frac{t_a^*}{t_c^*} \ll O(\epsilon). \tag{6}$$

The complete non-dimensional equations describing the physical system in figure 1 are identical to those in the previous study by Wang & Kassoy (1990*a*),

$$p = \rho T, \tag{7}$$

$$\rho_t + (\rho u)_x = 0, \tag{8}$$

$$\rho(u_t + uu_x) = -\frac{p_x}{\gamma} + \delta_3^4(\mu u_x)_x, \tag{9}$$

$$\rho(T_t + uT_x) = -(\gamma - 1)\, pu_x + \delta\left[\frac{\gamma}{Pr}(kT_x)_x + \tfrac{4}{3}\gamma(\gamma-1)\,\mu u_x^2\right], \tag{10}$$

where it has been assumed that the specific heats are constants. The subscripts t and x denote partial derivatives. The non-dimensional variables are defined in terms of dimensional quantities (with asterisk) by

$$\left.\begin{aligned} \rho &= \frac{\rho^*}{\rho_0^*}, \quad p = \frac{p^*}{p_0^*}, \quad T = \frac{T^*}{T_0^*}, \quad u = \frac{u^*}{c_0^*}, \\ t &= \frac{t^*}{t_a^*}, \quad x = \frac{x^*}{L^*}, \quad \mu = \frac{\mu^*}{\mu_0^*}, \quad k = \frac{k^*}{k_0^*}, \end{aligned}\right\} \tag{11}$$

where μ^* and k^* represent the dynamic viscosity and thermal conductivity respectively. The parameter γ is the ratio of specific heats and

$$\delta = \frac{t_a^*}{t_c^*} Pr, \quad Pr = \frac{C_{p0}^* \mu_0^*}{k_0^*}, \tag{12}$$

where the former is typically a quantity of $O(10^{-6})$.

The dynamic boundary conditions on the solid surfaces can be written as

$$x = X_p(t); \quad u = \frac{\mathrm{d}X_p(t)}{\mathrm{d}t} \equiv \epsilon \bar{U}_p(t), \tag{13}$$

$$x = 1; \qquad u = 0, \tag{14}$$

where $X_p(t)$ is the piston location and $\bar{U}_p(t)$ the scaled piston speed that is of order unity. The initial conditions consist of mean field and $O(\epsilon)$ disturbance quantities,

$$\left.\begin{aligned} u(t=0) &= \epsilon u_i(x), \quad p(t=0) = 1 + \epsilon p_i(x) \\ \rho(t=0) &= 1 + \epsilon \rho_i(x), \quad T(t=0) = 1 + \epsilon T_i(x) \end{aligned}\right\} \quad \text{for} \quad 0 < x < 1, \tag{15}$$

where u_i, p_i, ρ_i and T_i are of order unity. A typical piston Mach number considered is $\epsilon = O(0.05)$.

Solutions to the basic system (7)–(10) are to be sought in the limit $\epsilon \to 0, \delta \to 0$ where it is noted that $\delta \ll \epsilon$ according to assumptions made in (6). The limiting forms of (9) and (10) imply that the most important physical processes in the cylinder can be described by the inviscid, non-conducting versions of (9) and (10). In this respect, the state, continuity and energy equations can be combined to yield the familiar results

$$p = \rho^{\gamma} + O(\delta), \quad T = \rho^{\gamma-1} + O(\delta). \tag{16}$$

It follows from (9) that the momentum equation can be written as

$$\rho(u_t + uu_x) = -\rho^{\gamma-1}\rho_x + O(\delta). \tag{17}$$

As is pointed out in our previous study (Wang & Kassoy 1990*a*), transport effects may be important in very narrow regions, including shock waves and accommodation layers adjacent to solid surfaces described by Rott (1980), where the gas experiences steep changes in its velocity and other gasdynamic properties. The simplified non-dissipative system can be used to describe the physical processes everywhere in the system except inside those regions. Also, the present one-dimensional study is concentrated on the explicit effects of gasdynamic processes on equilibrium compression and expansion. In this sense the effect of non-planar flow (e.g. vortices and turbulence) are not addressed, although they inevitably occur in realistic situations.

For this constant-mass system the analysis is carried out conveniently by using a Lagrangian spatial variable,

$$s = \int_{X_p(t)}^{x} \rho(\hat{x}, t)\, \mathrm{d}\hat{x}. \tag{18}$$

The piston surface $x = X_p(t)$ is represented by $s = 0$, while the fixed endwall corresponds to $s = 1$ as a result of mass conservation, since the total mass of the dimensionless system is unity. Once s and t are used as new independent variables in place of the Eulerian variables x and t, (8) and (17) become

$$\rho_t + \rho^2 u_s = 0, \quad u_t + \rho^{\gamma-1}\rho_s = O(\delta). \tag{19}$$

The appropriate initial conditions are derived from (15):

$$u(t=0) = \epsilon u_i(s), \quad \rho(t=0) = 1 + \epsilon\rho_i(s), \tag{20}$$

while the boundary conditions take the form

$$s = 0; \quad u = \epsilon \bar{U}_p(t), \quad s = 1; \quad u = 0. \tag{21}$$

Once ρ and u are obtained, the pressure and temperature are found from the results in (16).

3. General solutions

The fast and slow time variables employed in the earlier study by Wang & Kassoy (1990*a*),

$$\tilde{t} = \int_0^t \rho_0^{\frac{1}{2}(\gamma+1)}(\epsilon\hat{t})\, \mathrm{d}t, \quad \tau = \epsilon t, \tag{22}$$

are employed here again to help describe acoustic and bulk phenomena in the gas. The former is basically the adjusted acoustic time, based on the instantaneous

distance between the piston and the endwall. The latter is the dimensionless time measured in terms of piston passage time, $\tau = t^*/t_p^*$. In (22) ρ_0 is the spatially homogeneous leading-order density of the gas defined by the asymptotic expansion

$$\rho = \rho_0(\tau) + \epsilon\rho_1 + \epsilon^2\rho_2 + \ldots. \tag{23}$$

Additionally, u is assumed to be described by

$$u = \epsilon u_1 + \epsilon^2 u_2 + \ldots. \tag{24}$$

A multiple-timescale formulation is employed by using the relation

$$\left(\frac{\partial}{\partial t}\right)_s = \rho_0^{\frac{1}{2}(\gamma+1)}\left(\frac{\partial}{\partial \tilde{t}}\right)_{\tau,s} + \epsilon\left(\frac{\partial}{\partial \tau}\right)_{\tilde{t},s}. \tag{25}$$

The expansions in (23), (24) as well as (25) can be inserted into the governing equations (19) to find an ordered set of equations in powers of ϵ. The first- and second-order equations are

$$\rho_0^{\frac{1}{2}(\gamma+1)}\rho_{1\tilde{t}} + \rho_0^2 u_{1s} = -\rho_0'(\tau), \tag{26}$$

$$\rho_0^{\frac{1}{2}(\gamma+1)}u_{1\tilde{t}} + \rho_0^{\gamma-1}\rho_{1s} = 0, \tag{27}$$

$$\rho_0^{\frac{1}{2}(\gamma+1)}\rho_{2\tilde{t}} + \rho_0^2 u_{2s} = -\rho_{1\tau} - 2\rho_0\rho_1 u_{1s}, \tag{28}$$

$$\rho_0^{\frac{1}{2}(\gamma+1)}u_{2\tilde{t}} + \rho_0^{\gamma-1}\rho_{2s} = -u_{1\tau} - (\gamma-1)\rho_0^{\gamma-2}\rho_1\rho_{1s}. \tag{29}$$

From (26), (27) it follows that the leading-order velocity field is described by

$$u_{1\tilde{t}\tilde{t}} = u_{1ss}, \tag{30}$$

which is subject to boundary conditions derived from (21):

$$s = 0; \quad u_1 = \bar{U}_p(\tau), \qquad s = 1; \quad u_1 = 0. \tag{31}$$

The general solution to (30), (31) can be put into the form

$$u_1 = (1-s)\,\bar{U}_p(\tau) + \sum_{n=1}^{\infty}[\alpha_n(\tau)\cos(n\pi\tilde{t}) + \beta_n(\tau)\sin(n\pi\tilde{t})]\sin(n\pi s). \tag{32}$$

The results can be used in (26) to obtain

$$\rho_0^{\frac{1}{2}(\gamma+1)}\rho_{1\tilde{t}} = [\rho_0^2(\tau)\,\bar{U}_p(\tau) - \rho_0'(\tau)] - \rho_0^2\sum_{n=1}^{\infty} n\pi[\alpha_n(\tau)\cos(n\pi\tilde{t}) + \beta_n(\tau)\sin(n\pi\tilde{t})]\cos(n\pi s). \tag{33}$$

In order that ρ_1 be bounded for any large $\tilde{t}$, it is required that

$$\rho_0' = \rho_0^2\,\bar{U}_p(\tau). \tag{34}$$

The basic density variation can be found from (34) and the appropriate initial condition, $\rho_0(\tau \to 0) = 1$,

$$\rho_0 = \frac{1}{1 - X_p(\tau)}, \tag{35}$$

where

$$X_p(\tau) = \int_0^{\tau} \bar{U}_p(\hat{\tau})\,\mathrm{d}\hat{\tau} \tag{36}$$

is the displacement of the piston. Equation (35) describes the slow-time variation of the basic, spatially homogeneous density caused by the changing cylinder volume.

This zeroth-order solution is equivalent to those obtained by Klein & Peters (1988) and Schneider (1981). It is also identical to the result from quasi-static thermodynamic calculations.

The first-order density ρ_1 is now derived from (27), (33) and (34),

$$\rho_1 = \rho_0^{\frac{1}{3}(3-\gamma)}\left\{\beta_0(\tau)+\sum_{n=1}^{\infty}\left[-\alpha_n(\tau)\sin(n\pi\tilde{t})+\beta_n(\tau)\cos(n\pi\tilde{t})\right]\cos(n\pi s)\right\}, \tag{37}$$

where $\beta_0(\tau)$ is the zeroth-order Fourier coefficient arising from indefinite integration. The functional forms of β_0, α_n and β_n are indeterminate at this stage of the analysis, as is typical for the method of multiple scales.

Initial conditions for the first-order quantities, obtained from (20), (23) and (24) are

$$\tilde{t} = \tau = 0; \quad u_1 = u_{1i}(s), \quad \rho_1 = \rho_{1i}(s). \tag{38}$$

These are substituted into (32) and (37) to give

$$\left.\begin{aligned}(1-s)\,\bar{U}_p(0)+\sum_{n=1}^{\infty}\alpha_n(0)\sin(n\pi s) &= u_{1i}(s),\\ \beta_0(0)+\sum_{n-1}^{\infty}\beta_n(0)\cos(n\pi s) &= \rho_{1i}(s).\end{aligned}\right\} \tag{39}$$

Consequently, initial values for α_n, β_n and β_0 are obtained from initial disturbances of the gas through Euler's formula for Fourier coefficients,

$$\left.\begin{aligned}\alpha_n(0) &= 2\int_0^1 [u_{1i}(s)-(1-s)\,\bar{U}_p(0)]\sin(n\pi s)\,\mathrm{d}s,\\ \beta_n(0) &= 2\int_0^1 \rho_{1i}(s)\cos(n\pi s)\,\mathrm{d}s,\end{aligned}\right\} \quad n = 1,2,\ldots, \tag{40}$$

$$\beta_0 = \int_0^1 \rho_{1i}(s)\,\mathrm{d}s. \tag{41}$$

The time variations of β_0, α_n and β_n are found from higher-order equations, by following a procedure identical to that used by Wang & Kassoy (1990*a*). The major steps and results are outlined below.

The second-order velocity equation is derived from (28), (29) and (34),

$$u_{2\tilde{t}\tilde{t}}-u_{2ss} = 2\rho_0^{-2}[\rho_{1\tau}+\tfrac{1}{4}(\gamma-7)\,\bar{U}_p(\tau)\,\rho_0\rho_1]_s-\tfrac{1}{2}(\gamma+1)\,\rho_0^{\frac{1}{3}(\gamma-5)}(\rho_1^2)_{s\tilde{t}}. \tag{42}$$

The right-hand side of (42) is evaluated using (37), and the resonant terms proportional to $\sin(n\pi\tilde{t})\sin(n\pi s)$ or $\cos(n\pi\tilde{t})\sin(n\pi s)$ are subsequently eliminated. This leads to secular equations for α_k and β_k,

$$\left.\begin{aligned}\alpha_k' &= \tfrac{1}{16}(\gamma+1)\,\rho_0[4\bar{U}_p(\tau)\,\alpha_k+k\pi(8\beta_0\beta_k+2c_k-e_k)],\\ \beta_k' &= \tfrac{1}{16}(\gamma+1)\,\rho_0[4\bar{U}_p(\tau)\,\beta_k+k\pi(-8\beta_0\alpha_k+2d_k-f_k)],\end{aligned}\right\} \quad k = 1,2,\ldots. \tag{43}$$

The quantities c_k, d_k, e_k and f_k in (43) are Fourier mode coupling terms,

$$\left.\begin{aligned}c_k &= \sum_{m=1}^{\infty}(\alpha_n\alpha_{n+k}+\beta_n\beta_{n+k}), \quad d_k = \sum_{n=1}^{\infty}(\alpha_n\beta_{n+k}-\alpha_{n+k}\beta_n),\\ e_k &= \sum_{n=1}^{k-1}(\alpha_k\alpha_{k-n}-\beta_k\beta_{k-n}), \quad f_k = \sum_{n=1}^{k-1}(\alpha_{k-n}\beta_n+\alpha_n\beta_{k-n}),\end{aligned}\right\} \tag{44}$$

where $e_1 = f_1 = 0$.

The first term on the right-hand side of each equation in (43) indicates the influence of piston velocity on the behaviour of the Fourier coefficients and, consequently, the acoustic disturbances (cf. (32) and (37)). The terms proportional to β_0 are caused by $O(\epsilon)$ corrections to the spatially uniform density of the gas. The last two terms are responsible for the development of nonlinear phenomena in the physical system. They are similar to the mode coupling terms in Ochmann's (1985) equation (40) for the complex amplitude function, which does not contain any effect of the changing average state.

The results in (34), (37), (42) and (43) can be utilized to evaluate (28). This gives (a detailed derivation can be found in the dissertation by Wang 1989)

$$\rho_0^{\frac{1}{2}(\gamma+1)}\rho_{2\tilde{t}} = -\rho_0^{\frac{1}{2}(3-\gamma)}[\beta_0' - \tfrac{1}{2}(\gamma+1)\rho_0 \bar{U}_p(\tau)\beta_0] + \text{non-secular terms}. \tag{45}$$

Equation (45) has the same form as (33) in the sense that both indicate the source of $O(\tilde{t})$ growth in densities. The same argument employed previously can be used to show that

$$\beta_0' = \tfrac{1}{2}(\gamma+1)\rho_0 \bar{U}_p(\tau)\beta_0 \tag{46}$$

in order to guarantee a finite value of ρ_2 in the limit when $\tilde{t} \to \infty$. Equation (46) can be solved easily to give

$$\beta_0 = \beta_0(0)\exp\left[\tfrac{1}{2}(\gamma+1)\int_0^\tau \rho_0(\hat{\tau})\,\bar{U}_p(\hat{\tau})\,\mathrm{d}\hat{\tau}\right], \tag{47}$$

which can be integrated to find

$$\beta_0 = \beta_0(0)\,\rho_0^{\frac{1}{2}(\gamma+1)} \tag{48}$$

if (34) is used in the integrand. Here $\beta_0(0)$ is the initial value given in (41).

Given the value of β_0, then α_k and β_k can be evaluated from (43) together with initial conditions (40), using a numerical technique that will be described in detail later.

The solutions to the mathematical system (19)–(21) are now formally complete, and are summarized below:

$$u = \epsilon\left\{(1-s)\,\bar{U}_p(\tau) + \sum_{n=1}^{\infty}[\alpha_n(\tau)\cos(n\pi\tilde{t}) + \beta_n(\tau)\sin(n\pi\tilde{t})]\sin(n\pi s)\right\} + O(\epsilon^2), \tag{49}$$

$$\rho = \rho_0 + \epsilon\left\{\rho_0^2\beta_0(0) + \rho_0^{\frac{1}{2}(3-\gamma)}\sum_{n=1}^{\infty}[-\alpha_n(\tau)\sin(n\pi\tilde{t}) + \beta_n(\tau)\cos(n\pi\tilde{t})]\cos(n\pi s)\right\} + O(\epsilon^2). \tag{50}$$

As is expected, (49) and (50) resemble the piston time solutions given in our previous study (Wang & Kassoy 1990*a*). Nonetheless, the current results are greatly generalized because they are valid for arbitrary piston velocity and initial gas conditions. The first term in (49) and the first two terms in (50) represent the bulk effect of uniform compression and expansion of the gas due to piston motion. The summation terms are Fourier decomposed standing wave representations of the instantaneous acoustic field arising from the initially non-uniform distributions of velocity and density of the gas. The piston motion affects the evolution process of the wave field, while repeated passage of these waves contributes to the bulk variation

of the gas properties. One advantage of employing the Fourier series technique to solve the present problem is that it shows in an explicit manner the acoustic phenomenon, the bulk response of the gas, and the interactions between them.

In addition to gas velocity and density, it is also of interest to consider other thermodynamic properties. For example, temperature and pressure are more easily measured in a dynamic system. In the present analysis where the isentropic relations in (16) are valid, T and p can be found easily:

$$p = \rho_0^{\gamma} + \epsilon\gamma\rho_0^{\gamma-1}\rho_1 + O(\epsilon^2), \tag{51}$$

$$T = \rho_0^{\gamma-1} + \epsilon(\gamma-1)\,\rho_0^{\gamma-2}\rho_1 + O(\epsilon^2). \tag{52}$$

Qualitatively both the pressure and the temperature fields of the system exhibit variations similar to the density field. Since $\gamma > 1$ the basic pressure change is larger, and the temperature change smaller than the density change.

Before carrying out a numerical analysis for the equation system (43), (44), two simplified cases are worth considering. First, when the cylinder gas is initially static, or quasi-static with compatible boundary conditions on the piston face and the cylinder wall, $u_i = (1-s)\,\bar{U}_p(0), \rho_i = 0$, then according to (40), (41), $\beta_0(0) = 0$ and $\alpha_k(0) = \beta_k(0) = 0$ for $k = 1, 2, \ldots$. The solution to the homogeneous equation system (43), (44), obtained analytically, is $\alpha_k(\tau) = \beta_k(\tau) = 0$. This result illustrates that if no disturbance to the quasi-static gas field is present at the beginning, the system always remains static or quasi-static up to $O(\epsilon)$. The slow variation of piston velocity on the piston timescale does not create disturbances in the gas medium to the order considered here, in contrast to the case in the previous study by Wang & Kassoy (1990*a*) where an $O(\epsilon)$ acoustic disturbance is generated by piston acceleration that occurs on the much shorter acoustic timescale.

Secondly, (43), (44) can be greatly simplified if the initial disturbance is confined to the velocity profile. This simplification occurs because if $\rho_i = 0$, then $\beta_0(0) = \beta_k(0) = 0$ for $k = 1, 2, \ldots$. The second equation in (43) implies that $\beta_k(\tau) = 0$ because it is homogeneous with respect to β_k. The first equation for α_k will have a reduced form because all the β_k-related terms are dropped out. This simplified system, rather than the full system, will be used in subsequent calculations whenever the condition $\rho_1(s) = 0$ is satisfied.

4. Numerical results

4.1. *Numerical method and error analysis*

In order to obtain solutions for the velocity and thermodynamic properties of the gas in the cylinder. One must construct solutions to truncated forms of (49), (50) and use finite summations as approximate answers. If it is desired to add up N terms in the Fourier series, $2N$ coupled equations for α_k and β_k from (43) have to be solved. The infinite summations appearing in c_k and d_k in (44) have to be truncated at the $(N-k)$th Fourier mode in order to close the mathematical system. These truncations are based on the assumption that the geometric series of Fourier coefficients in (44) are convergent. This can be readily verified even for the severest case of discontinuous solutions in (49) and (50), for which both α_k and β_k behave like $1/k$.

The relative truncation errors introduced into the mathematical system can be estimated in the order-of-magnitude sense. Since α_k and β_k are of similar magnitude, either of the equations in (43) can be taken as the basis of evaluation. Since the series in (44) is convergent, the first neglected term should give an overall order-of-

magnitude estimation of the total truncation. Thus the truncation error of the kth equation is of $O(k\alpha_{N-k+1}\alpha_{N+1})$, while the largest term in the equation is of $O(k\alpha_1\alpha_{k+1})$. Consequently the relative truncation error of the kth equation is

$$E_k = O\left(\frac{\alpha_{N-k+1}\alpha_{N+1}}{\alpha_1\alpha_{k-1}}\right). \tag{53}$$

The k-dependence of the α_k, β_k coefficients and hence the convergence behaviour of a Fourier series are determined by the properties of the original function. According to Kufner & Kadlec (1971), $\alpha_k, \beta_k \sim 1/k$ for a function with discontinuities (such as a shock wave), while $\alpha_k, \beta_k \sim 1/k^2$ for a continuous function with discontinuous first derivative (such as a piston-generated acoustic wavefront (Wang & Kassoy 1990*a*, *b*)). It follows from (53) that

$$E_k = \begin{cases} O\left(\dfrac{k-1}{(N+1)(N-k+1)}\right) & \text{for shock case,} \\ O\left(\dfrac{(k-1)^2}{(N+1)^2(N-k+1)^2}\right) & \text{for shock-free case.} \end{cases} \tag{54}$$

Obviously, when k gets closer to N the truncated equations in (43), (44) become less accurate relative to those for small k-values. Terms with relatively large error are avoided by using only the first $\frac{1}{3}N$ to $\frac{2}{3}N$ Fourier modes in the series to calculate the velocity and density of the gas. The optimal number of modes is determined by numerical experimentation. It should be noted from (54) that the truncation error for a shock-free system is the square of that for an embedded shock system. As a result the numerical solutions are always reasonably accurate for continuous acoustic wave fields, while they become increasingly inaccurate once a shock is present. It should be pointed out that the preceding truncation-error analysis is based on each individual equation. In the numerical procedure $2N$ equations are integrated simultaneously, so that the errors tend to spread out among different Fourier coefficients. However, this effect is small because terms with relatively large errors are of small absolute magnitude.

Numerical integrations of the truncated version of equation system (43), (44) with initial conditions (40) are carried out by utilizing the DGEAR subroutine available in the IMSL computer software library. The subroutine is adapted from a package designed by Hindmarsh (1974) based on Gear's subroutine DIFSUB (Gear 1971). By proper choice of the input basic method indicator in DGEAR, the Adams methods (up to order twelve), which are basically of the implicit predictor-corrector type, are employed. This choice is suitable because the differential equation system is non-stiff. The corrector iteration method employed is of the functional iteration type. In the calculations that follow, the relative error tolerance per time step is set to be 10^{-6}, which is sufficiently small considering the intrinsic truncation errors in the approximate system. The truncation level is typically taken as $N = 300$, so that a total of 600 equations are solved simultaneously to obtain α_1–α_{300} and β_1–β_{300}. Among them between 100 and 200 terms are actually used in the Fourier summations in (49)–(52). Production runs were conducted on the satellite-linked CYBER 205 at the John Von Neumann Supercomputing Center in Princeton. It is important to mention here that the large number of terms were computed in order to attain sufficient resolution for shocks, and hence an accurate appraisal of the method in dealing with the shock. For practical purposes one can obtain cruder but

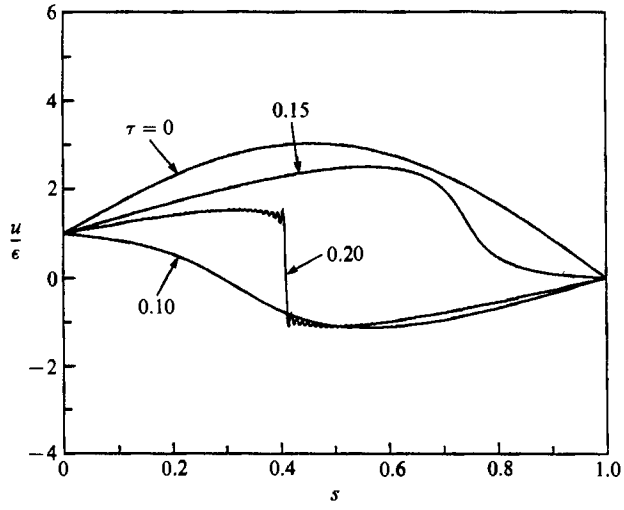

FIGURE 2. Velocity distributions in the Lagrangian coordinate s during piston time compression, $\bar{U}_p = 1$. The initial gas state is described by $u_i = 1 - s + \frac{5}{2}\sin(\pi s)$ and $\rho_i = 0$. The piston Mach number $\epsilon = 0.02$.

representative solutions with fewer Fourier modes (20 to 50 terms, say) without significant loss of accuracy, especially before shock formation. A VAX-class mainframe computer can well serve this purpose.

4.2. *Compression of an initial disturbance: comparison with Klein & Peters' results*

The general formulation developed in the present study can be applied easily to compression systems with a variety of initial and boundary conditions. In the example considered here, a cylinder of gas undergoing uniform compression by a constant-speed piston is perturbed by a sinusoidal velocity disturbance at an arbitrarily defined initial time instant. The piston velocity function and the initial conditions of the gas are described by

$$\left.\begin{aligned} \bar{U}_p(\tau) &= 1, \\ \rho_i(s) = 0, \quad u_i(s) &= 1 - s + \tfrac{5}{2}\sin(\pi s), \end{aligned}\right\} \tag{55}$$

which are equivalent to those used by Klein & Peters (1987 personal communication, 1988) in their studies of shock formation during cylinder compression, with the exception of a phase shift in the harmonic wave shape function. The initial velocity profile across the cylinder is shown as the uppermost curve in figure 2, where the curve section with negative (positive) slope is compressive (expansive). As time evolves the compressive part of the wave steepens to form a shock, while the expansive part flattens as the wave propagates back and forth in the cylinder. The process can be observed clearly from the other three velocity curves in figure 2 at $\tau = 0.10$, 0.15 and 0.20. At $\tau = 0.2$ the velocity curve becomes almost sawtooth-like. The piston Mach number used in the calculation is $\epsilon = 0.02$. Owing to the small ratio of the acoustic to piston timescale, several wave reflections have occurred between two neighbouring time instants depicted in the figure.

In figures 3 (a) and 3 (b) the temperature variations at the piston surface $s = 0$, and at the material point $s = \frac{1}{4}$, are depicted respectively. The alternating arrivals of the compression and expansion wave portions at the given location cause the temperature to oscillate around the bulk value, which is spatially uniform, and is

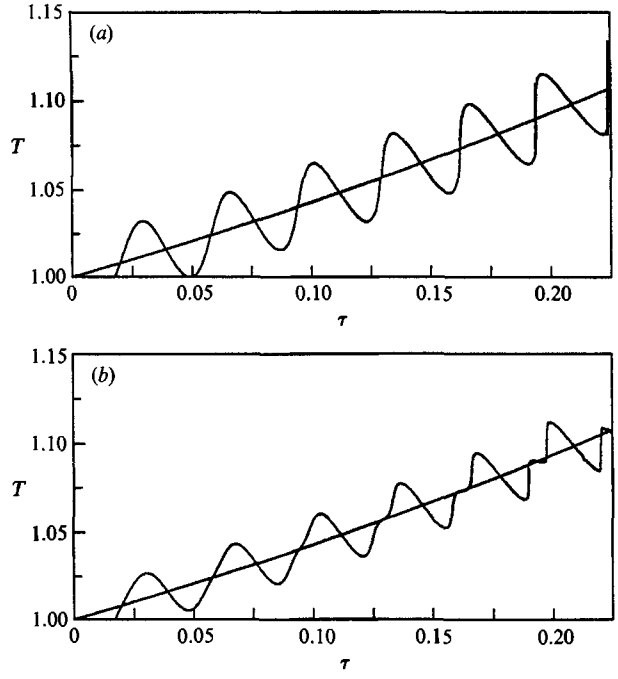

FIGURE 3. Temperature variations at specified material points s during piston time compression, $\bar{U}_p = 1$. The initial gas state is described by $u_i = 1 - s + \frac{5}{2}\sin(\pi s)$ and $\rho_i = 0$. The piston Mach number $\epsilon = 0.02$. Case (*a*) $s = 0$, case (*b*) $s = \frac{1}{4}$.

represented by the monotone increasing line in each figure. The gas temperature rises owing to compressive heating, and drops when thermal energy is converted into kinetic energy during the expansion phase. As the compression part of the wave steepens to form a shock, its passage time through the given location tends to zero, as is seen on the T–τ curves. Figure 3(*a*) is plotted under identical conditions to those of figure 4 in Klein & Peters' (1988) study. Good agreement is observed between both figures in terms of the wave deformation process and the shock formation time. A more quantitative comparison would require the phase value in Klein & Peters' initial wave shape function, which was not reported. The material point at $s = \frac{1}{4}$ (cf. figure 3*b*) experiences the same wave portion after it travels a round trip between the mass point and one of the solid boundaries. The two characteristic round-trip times are clearly visible after considerable steepening of the wavefront. They are not equal owing to the non-symmetric locations of the two confining boundaries relative to the given material point. The density and pressure at a given mass location will exhibit similar oscillatory variations with different amplitudes, as is anticipated from (51) and (52). Calculations are terminated shortly after the shock formation, when convergence properties of the truncated series begin to deteriorate. One can nonetheless observe clearly the tendency for the wave field to approach its asymptotic sawtooth shape.

In a compressing system the compressive wavefront always steepens to form a shock. The time for this process to occur is dependent upon the amplitude of the initial disturbance. Calculations with smaller initial velocity disturbance input show longer shock formation time.

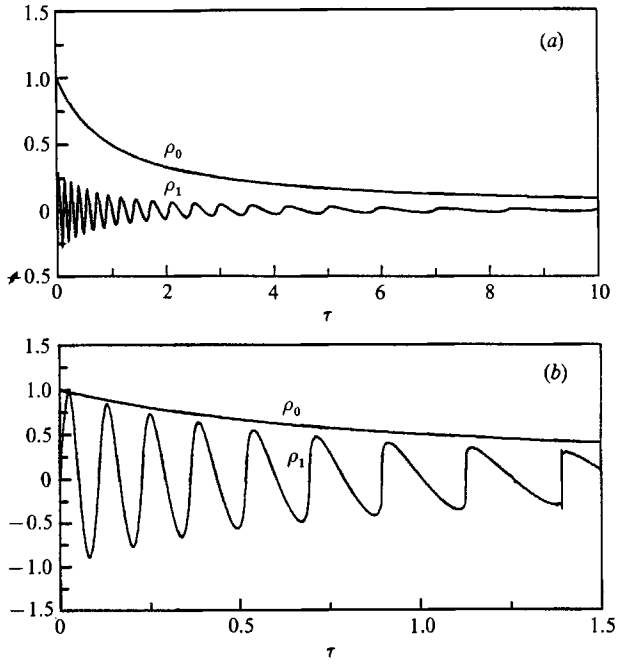

FIGURE 4. Zeroth- and first-order density variations of the gas on the piston surface, which moves out of the cylinder with constant velocity $\bar{U}_p = -1$. The initial gas state is described by $u_i = -(1-s) - h\sin(\pi s)$ and $\rho_i = 0$. The total density $\rho = \rho_0 + \epsilon\rho_1$. The piston Mach number $\epsilon = 0.05$. Case (*a*) $h = 0.3$, case (*b*) $h = 1.0$.

4.3. *Expansion of an initial disturbance*

The evolution of initial sinusoidal disturbances in an expanding environment is illustrated by a second example. Consider the case when the piston moves out of the cylinder at constant velocity, $\bar{U}_p = -1$. The initial disturbance of the gas is given by

$$u_i(s) = -(1-s) - h\sin(\pi s), \quad \rho_i(s) = 0, \tag{56}$$

where h is a constant reflecting the amplitude of the disturbance. If $|h| < 1/\pi$, $\mathrm{d}u_i/\mathrm{d}s$ is positive for any s-value, hence the initial acoustic wave is purely expansive. In this expansion system no shock wave can be formed owing to the lack of mechanisms to generate compressive regions in the gas. This is graphically demonstrated in figure 4(*a*), where the zeroth- and first-order density on the piston surface $s = 0$ are plotted with respect to time, for the case when $h = 0.3 < 1/\pi$ and $\epsilon = 0.05$. The oscillatory ρ_1 is caused by repeated reflections of the expansion wave on the piston face. The wave deformation is obviously seen in the figure but no shock formation is achieved. It is observed that the wave field is damped as the global expansion process proceeds. In the meantime, the wave-passage frequency decreases significantly owing to the extended distance between the piston face and the cylinder wall, as well as the reduced sound speed caused by gas temperature reduction associated with expansion.

If, on the other hand, $|h| > 1/\pi$, then the initial velocity profile $u_i(s)$ has two distinct portions, a compressive portion ($\mathrm{d}u_i/\mathrm{d}s < 0$) and an expansive portion ($\mathrm{d}u_i/\mathrm{d}s > 0$). Even during an expansion process the former part of the wave will steepen to form a shock. The results in figure 4(*b*) are for $h = 1.0$ and $\epsilon = 0.05$. In the present case the shock is formed at $\tau \approx 1.0$, after which the ρ_1–τ curve approaches

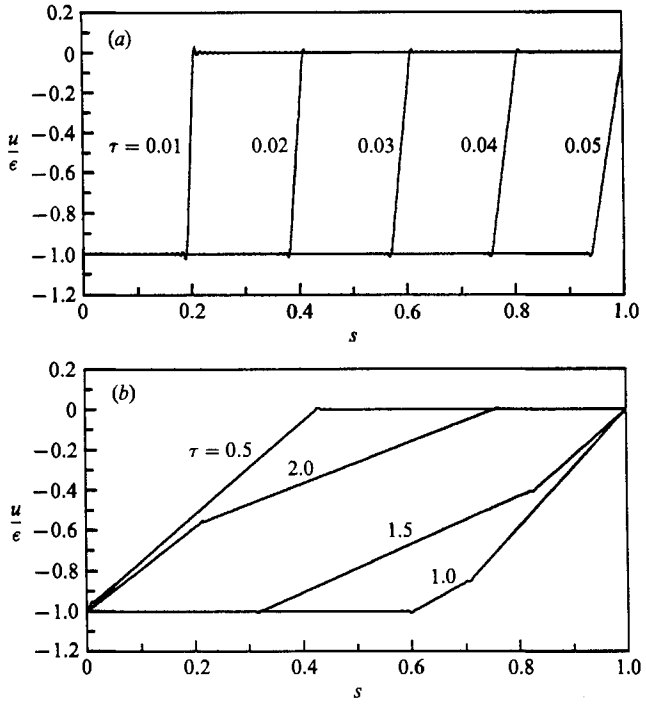

FIGURE 5. Velocity distributions in the Lagrangian coordinate s, generated by impulsively started backward piston motion $\bar{U}_p = -1$, in an initially static gas. The piston Mach number $\epsilon = 0.05$. (*a*) Short-time solutions, (*b*) solutions at more extended time.

sawtooth shape. The amplitude of the disturbance is found to decrease with increasing cylinder volume.

The next calculation describes the expansion in a gas due to impulsively started backward piston motion. The gas is initially at rest and in thermodynamic equilibrium: $u_1 = 0, \rho_1 = 0$. At $t = 0^+$ the piston begins to move away from the cylinder endwall with constant speed, $\bar{U}_p = -1$. The instantly generated gas flow consists of two regions of velocity -1 and 0 respectively, separated by a rightward-propagating rarefaction wave whose velocity varies linearly from -1 to 0. This is shown in figure 5(*a*), which presents the instantaneous velocity distributions of the gas in the Lagrangian coordinate, at some specified times prior to the first reflection of the rarefaction wave on the cylinder wall. The two boundaries of the rarefaction wave are weak discontinuities whose speeds of propagation are different from each other, which leads to a broadening of the rarefaction wave. The small oscillations observed at the two edges of the rarefaction wave are Gibbs effects, which are related to the steepness of the rarefaction wave. It disappears gradually as the rarefaction wave flattens out. Before the rarefaction wave reaches the opposite cylinder endwall, the flow field of the gas is identical to that in a semi-infinite cylindrical pipe considered by Landau & Lifshitz (1959), where analytical solutions are given. In the later development of the wave field, the two weak discontinuities are reflected repeatedly from the solid boundaries. The distance in between may become so long that the rarefaction wave can no longer be identified as a whole in the cylinder. This situation is depicted in figure 5(*b*), for the velocity distributions at more extended times. In this figure the time intervals between two neighbouring curves are so long

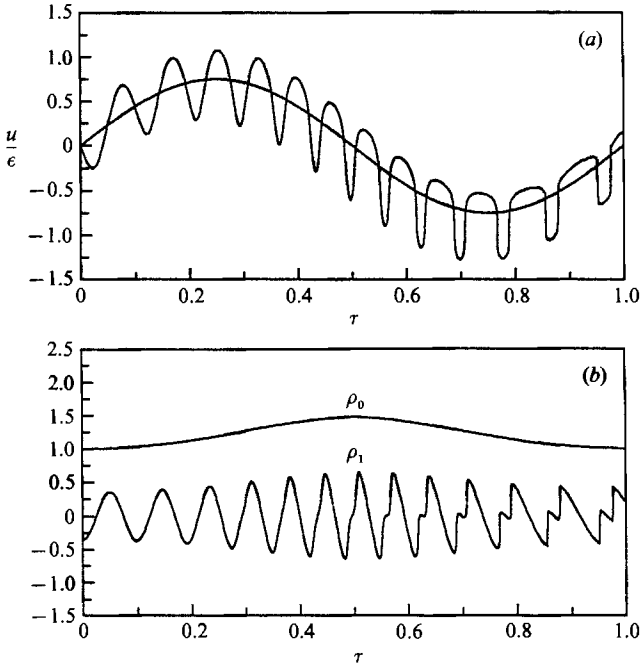

FIGURE 6. Velocity and density variations at specified material point $s = \frac{1}{4}$, in a cylinder gas subject to piston motion $\bar{U}_p = \sin(2\pi\tau)$. The initial gas state is described by $\rho_i = -0.5\cos(\pi s)$ and $u_i = 0$. The maximum piston Mach number $\epsilon = 0.05$. (*a*) Velocity, (*b*) zeroth- and first-order density.

that one can no longer follow the propagation of the rarefaction wave, as is the case in figure 5(*a*). The boundaries of the rarefaction wave can still be identified clearly as the points of discontinuous slopes. The time variations of density and velocity at any spatial location can also be easily plotted.

4.4. *Periodic piston motion*

The response of a confined gas to periodic piston motion is of practical interest because of its relevance to reciprocating engines. In the case considered here, the piston velocity is given by $\bar{U}_p = \sin(2\pi\tau)$. The initial density disturbance is defined by $\rho_i = -0.5\cos(\pi s)$, while the initial velocity is zero, so that it is compatible with the piston speed at $\tau = 0$. The cases of unequal piston-gas velocities at the interface are considered in §§4.3 and 5 respectively. The maximum piston Mach number considered here is $\epsilon = 0.05$.

The result shown in figure 6(*a*) is for the velocity variation with time at the Lagrangian coordinate $s = \frac{1}{4}$. The slowly varying curve with period 1 is the average velocity of the material point, and the rapidly fluctuating curve represents the actual velocity of the point due to the acoustic field. Initially, owing to the positive density and pressure gradients at $s = \frac{1}{4}$, the gas particle tends to flow in the negative direction until the other portion of the density disturbance of negative gradient reaches this location and reverses the flow direction. At later times as the disturbance travels back and forth in the cylinder, the velocity of the gas fluctuates correspondingly around its bulk mean value. The zeroth- and first-order density variations with τ at the same location are given in figure 6(*b*). The amplitude of the density disturbance increases during the compression stroke, owing to the rising bulk density, as is expected from (50). During the expansion stroke the reversed effect is observed. The

wave-passage frequency increases with ρ_0, owing to both the reduced wave travelling distance and the increased sound speed. One observes that the global expansion of the gas during the expansion stroke of the piston does not prevent the shock formation process. After the shock is formed and the wave tail is flattened, one observes in figure 6 abrupt changes in u and ρ_1 with time as the shock passes the given location, followed by slow variations of the two quantities as the wave tail travels through. The wave shape again approaches a sawtooth. The effect of two different characteristic round-trip times between the given mass point and the two confining solid walls, is again clearly observed in figure 6 after the shock formation. Calculations with various initial conditions also show longer shock formation time for smaller amplitude waves.

The example calculations carried out in §4 have demonstrated the effectiveness of the Fourier series technique in describing acoustic wave evolution in both compression and expansion processes. The numerical solutions, however, become unsatisfactory soon after the shock appears in the system, owing to large truncation errors in approximating the infinite equation system (43), (44). In the next section we concentrate on a special class of shock waves, the so-called 'standing sawtooth wave', which is the long-time asymptotic behaviour of the general shock wave fields considered above. For this type of wave the infinite system (43), (44) can be solved without truncation, and hence excellent results are obtainable.

5. Piston-driven sawtooth waves

5.1. *Standing sawtooth wave*

It is well known that as a result of nonlinear convective distortion, a compressive acoustic wave of finite amplitude propagating in a semi-infinite space has an asymptotic waveform of a sawtooth (Whitham 1974), often referred to as a simple sawtooth wave. In a finite geometry standing waves can be thought of as superpositions of counter-propagating travelling waves (Ochmann 1985; Klein & Peters 1988). As a result, one can think of the asymptotic form of a standing wave as a superposition of simple sawtooth waves travelling in opposite directions, provided that no external excitations are applied to the wave system.

If external excitations are imposed on the system, on a timescale long compared with its acoustic timescale, the limiting waveform after the shock formation is also sawtooth-like, as evidenced in the calculations of Schneider (1981), Klein & Peters (1988) and those in §4 of the present paper. Chu (1963) discusses another interesting case where the standing sawtooth wave is present, and provides a graphical illustration of the waveform. It consists of two lines of identical slope separated by a travelling shock which is repeatedly reflected from both solid walls.

On the other hand, if the gas column is driven externally on the acoustic timescale, as in the resonant studies conducted by Betchov (1958) and Chester (1964), the limiting-cycle behaviour of the gas motion reflects the characteristics of the piston motion, and is thus not sawtooth-like. This class is irrelevant to the present work.

Travelling sawtooth waves can be represented easily in terms of Fourier series. A treatment of this type is given by Temkin (1969), where the acoustic velocity and pressure fields inside a tube are written as Fourier-decomposed standing sawtooth waves, obtained by superposing identical leftward- and rightward-running trains of sawtooth waves with a wavelength twice the tube length (cf. equations (15)–(17) in Temkins's study). The resulting expressions are quite simple and compact. It is important to point out, though, that the velocity expressions in Temkins's paper

must be multiplied by -1 in order to satisfy Euler equations and the entropy condition for the gasdynamic system. Additionally, the corresponding graphical illustrations must be altered appropriately. As presented they actually represent a spurious rarefaction shock, not compatible with the given pressure expression.

The compactness of Fourier series representations of sawtooth waves suggests to us that great simplification may be achieved for the general results derived in §3, if they are applied to sawtooth waves in the piston driven cylinder gas.

5.2. *Derivation of shock equations*

We consider a sawtooth velocity field with velocity jump $A_i = u_i(s=0^-) - u_i(s=0^+) > 0$ and compatible density jump in the cylinder. The discontinuity is assumed to be located initially on the piston surface $s=0$ to simplify the analysis, although cases with arbitrary initial shock position can also be treated by incorporating a phase angle in the subsequent derivations. Specification of the initial shock position at $s=0$ imposes no important restrictions on the generality of the problem. It is an exact representation of the case when the shock is generated instantaneously by an impulsively started piston. For shocks formed after long-time evolution, it should always be possible to choose the starting point of an analysis as the time at which the shock lies against the piston face.

Given the piston velocity $\bar{U}_p(\tau)$ and the gas velocity jump A_i adjacent to the piston face, the initial velocity field of the gas is described by the linear profile

$$u_i = [\bar{U}_p(0) - A_i](1-s). \tag{57}$$

If the shock is initiated by an impulsive piston motion, then $A_i = \bar{U}_p(0)$ and $u_i = 0$. The compatible initial density field is uniform everywhere except for an abrupt change on the piston face where the shock is present. Thus $\rho_i = 0$. From (40), (41), (43) and (48) one finds that $\beta_0(\tau) = 0$ and $\beta_k(\tau) = 0$ for $k = 1, 2, \ldots$. The differential equations for α_k are reduced to

$$\alpha_k' = \tfrac{1}{16}(\gamma+1)\rho_0\left[4\bar{U}_p\alpha_k + k\pi\left(2\sum_{n=1}^{\infty}\alpha_n\alpha_{k+n} - \sum_{n=1}^{k-1}\alpha_n\alpha_{k-n}\right)\right], \quad k = 1, 2, \ldots, \infty, \tag{58}$$

where the last summation is equal to zero when $k=1$. The initial conditions for α_k are obtained from (57) and the first equation in (40),

$$\alpha_k(0) = -\frac{2}{k\pi}A_i. \tag{59}$$

The form of (59) suggests that solutions of the type

$$\alpha_k = -\frac{2}{k\pi}A(\tau) \tag{60}$$

are useful. Equation (60) can be used in (58) to find

$$A'(\tau) = \tfrac{1}{4}(\gamma+1)\rho_0[\bar{U}_p(\tau)A(\tau) - A^2(\tau)k^2S_k], \quad k = 1, 2, \ldots, \infty, \tag{61}$$

where

$$S_k = \begin{cases} \displaystyle\sum_{n=1}^{\infty}\frac{1}{n(n+1)}, & k = 1, \\ \displaystyle\sum_{n=1}^{\infty}\frac{1}{n(n+k)} - \sum_{n=1}^{k-1}\frac{1}{2n(k-n)}, & k = 2, 3, \ldots, \infty. \end{cases} \tag{62}$$

It can be proved easily, using the method of mathematical induction, that

$$S_k = \frac{1}{k^2}. \tag{63}$$

As a consequence, (61) becomes k-independent. The resulting equation for $A(\tau)$ and the corresponding initial condition can be written as

$$\frac{\mathrm{d}A}{\mathrm{d}\tau} = \tfrac{1}{4}(\gamma+1)\rho_0 A(\tau)[\bar{U}_\mathrm{p}(\tau) - A(\tau)], \tag{64}$$

$$A(\tau = 0) = A_\mathrm{i}. \tag{65}$$

Equations (60) and (64) define a nonlinear mathematical system equivalent to the infinite system (58). The new describing system is enormously simpler than the old one because it has no coupling between different Fourier modes. Nonetheless it has some of the nonlinear features of the old system. By solving a single-amplitude equation, (64), one can obtain the Fourier coefficients to any order. Since no truncation is made in the derivation of (64), the resulting Fourier series is guaranteed to converge, and excellent results can be obtained to resolve the shock propagation in the cylinder for any period of time.

The velocity and density of the gas, obtained by combining (49), (50) and the preceding results of this section, take the form,

$$u = \epsilon\left[(1-s)\,\bar{U}_\mathrm{p}(\tau) - A(\tau)\sum_{k=1}^{\infty}\frac{2}{k\pi}\cos(k\pi\tilde{t})\sin(k\pi s)\right] + O(\epsilon^2), \tag{66}$$

$$\rho = \rho_0 + \epsilon[\rho_0^{\frac{1}{2}(3-\gamma)}A(\tau)]\sum_{k=1}^{\infty}\frac{2}{k\pi}\sin(k\pi\tilde{t})\cos(k\pi s) + O(\epsilon^2). \tag{67}$$

The pressure and temperature of the gas are calculated subsequently from the density field via (51) and (52),

$$p = \rho_0^{\gamma} + \epsilon[\gamma\rho_0^{\frac{1}{2}(\gamma+1)}A(\tau)]\sum_{k=1}^{\infty}\frac{2}{k\pi}\sin(k\pi\tilde{t})\cos(k\pi s) + O(\epsilon^2), \tag{68}$$

$$T = \rho_0^{\gamma-1} + \epsilon[(\gamma-1)\rho_0^{\frac{1}{2}(\gamma-1)}A(\tau)]\sum_{k=1}^{\infty}\frac{2}{k\pi}\sin(k\pi\tilde{t})\cos(k\pi s) + O(\epsilon^2). \tag{69}$$

Equations (66)–(69) are Fourier sine and cosine series representations of velocity and thermodynamic properties of the gas, respectively. Each Fourier summation represents a standing sawtooth wave, which can be decomposed into identical rightward- and leftward-travelling simple sawtooth waves of length 2. For example, (66) can be put into the form

$$\frac{u}{\epsilon} = (1-s)\,\bar{U}_\mathrm{p}(\tau) - A(\tau)\sum_{k=1}^{\infty}\frac{1}{k\pi}\{\sin[k\pi(s-\tilde{t})] + \sin[k\pi(s+\tilde{t})]\}. \tag{70}$$

The same treatment can be applied to equations for ρ, p and T. Equations (66)–(70), obtained through rigorous mathematical derivations, are seen to be similar to those 'suggested' by Temkin (1969).

Given (70), the lowest-order shock path lies either on the characteristic lines $s-\tilde{t}$ = const. or on $s+\tilde{t}$ = const., because its direction of propagation is reversed each time it hits the confining walls at $s = 1$ and $s = 0$ (see figure 7). The shock path

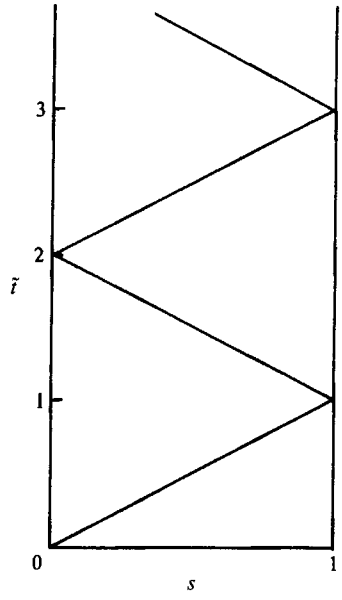

FIGURE 7. Path of the shock wave generated by impulsive piston motion, in the Lagrangian coordinate s.

divides the $(\tilde{t}, s)$-plane into triangular regions, each with continuous velocity and thermodynamic properties. This agrees to the leading order with calculations based on the method of characteristics, where the path of the weak shock is usually constructed from the boundaries of the multivalued regions using the bisector rule (Kluwick 1981; Klein & Peters 1988).

The height of each sawtooth is modulated by the τ-dependent group of parameters in front of the summation. One obtains from (66)–(69)

$$[u] = \pm \epsilon A(\tau), \qquad [\rho] = \epsilon \rho_0^{\frac{1}{2}(3-\gamma)} A(\tau),$$
$$[p] = \epsilon \gamma \rho_0^{\frac{1}{2}(\gamma+1)} A(\tau), \quad [T] = \epsilon(\gamma-1)\rho_0^{\frac{1}{2}(\gamma-1)} A(\tau), \tag{71}$$

where [ ] denotes the jump of a quantity across the shock. In the above expression for $[u]$ the positive (negative) sign corresponds to the case when the shock propagates in the positive (negative) direction. The conventional definition of the shock strength z is given by

$$z \equiv \frac{[p]}{p_0} = O(\epsilon), \tag{72}$$

where $p_0 = \rho_0^\gamma$ is the spatially homogeneous pressure term in (68). With this definition, the shock conditions (71) can be expressed in terms of normalized values:

$$\frac{[u]}{c_0} = \pm\frac{z}{\gamma} + O(z^2), \quad \frac{[\rho]}{\rho_0} = \frac{z}{\gamma} + O(z^2), \quad \frac{[T]}{T_0} = \frac{\gamma-1}{\gamma} z + O(z^2), \tag{73}$$

where $T_0 = \rho_0^{\gamma-1}$ is the $O(1)$ spatially homogeneous temperature, $c_0 = \rho_0^{\frac{1}{2}(\gamma-1)}$ is the dimensionless sound speed of the mean field, which is to order ϵ also the propagation speed of the shock. Relations (73) are, to first order in the shock strength, in agreement with the jump conditions given by the Rankine–Hugoniot law for weak

shocks (Whitham 1974), although they are derived directly from the non-dissipative Euler equations. Equations (73) also prove that (66)–(69) are indeed weak solutions to the Euler equations, because their continuous parts satisfy the differential equations, and their jump values across the discontinuity satisfy jump conditions derived from the equations.

5.3. *Fundamental solutions*

Solutions to the gasdynamic system require the evaluation of $A(\tau)$, governed by (64), (65). A discussion of (64) and its two fundamental solutions is presented here first, to relate the present work with earlier investigations, and to provide clearer physical interpretations for the general solution to be given in §5.4.

It is noted that positive $A(\tau)$ values represent compressive shocks, while negative $A(\tau)$ values correspond to discontinuous rarefaction waves or rarefaction shocks. Although the jump conditions (73) are satisfied by both types of discontinuities, rarefaction shocks are not admitted in physical systems because they cause the entropy of the gas particles to decrease (Lax 1973; Smoller 1983). As long as $A_1 > 0$, $A(\tau)$ is expected to be positive-definite, to ensure physically meaningful solutions. Thus from (64) it is clear that $A(\tau)$ tends to increase when $A(\tau) < \bar{U}_p(\tau)$, and decrease when $A(\tau) > \bar{U}_p(\tau)$. The rate of change in $A(\tau)$ is proportional to the mean density field.

Two fundamental solutions of (64), (65) are obtained immediately:

(i) *Solution for* $\bar{U}_p \equiv 0$

This case corresponds to a shock propagating in a constant-volume cylinder with zero external force. In this case $\rho_0 = 1$, and (64) agrees with Ochmann's (1985) equation (46) in the absence of transport effects, where it is recognized that $h = \theta A$. Equation (64) can be integrated easily to give

$$\frac{1}{A} - \frac{1}{A_1} = \tfrac{1}{4}(\gamma+1)\tau, \tag{74}$$

where $\tau = \epsilon t$ is the dimensionless time based on the characteristic time of convective gas motion, since there is no characteristic piston time in this constant-volume cylinder. The above relation shows how the velocity jump across the shock decreases with time from its initial value A_1. The long-time behaviour of A is inversely proportional to τ. By employing the shock relations in (73), (74) may be rewritten as

$$\frac{1}{z} - \frac{1}{z_i} = \frac{\gamma+1}{4\gamma}\chi, \tag{75}$$

to describe the damping of the shock strength. Here $\chi = t$ is the total distance travelled by the shock wave before its strength decreases from z_i to z. Relations (74) and (75) can also be derived conveniently by application of the combined bisector and area rules, described by Whitham (1974) and Lighthill (1978), to the sawtooth wave.

Since no energy exchange exists between the static piston and the wave field, the decay of the shock can only be a result of the accumulated dissipation effect inside the shock. It is important to point out that weak solutions of the Euler equations *do* contain energy dissipation across the discontinuity, because the isentropic relations are satisfied only on the continuous parts of the solution. The jump conditions (72), (73) determine the dissipation of acoustic energy by the shock, even without

knowledge of its internal structure. It is noted that (75) has a form identical to the classical formula describing the attenuation of repeated shock waves of wavelength 2 propagating in an infinite medium (Morse & Ingard 1968). The latter is derived based on the argument that the rate of entropy increase across the shock must be at the expense of the acoustic energy. The shock reflections on rigid boundaries are thus seen to have no effect on its energy loss.

(ii) *Solution for* $A_i = \bar{U}_p(\tau) \equiv 1$

This corresponds to the well-known case of an impulsively started, constant-velocity piston motion into an initially undisturbed gas. In this case the solution to the system (64), (65) is $A(\tau) = 1$. A shock wave propagates back and forth inside the cylinder, separating two homogeneous regions of velocity 1 and 0 respectively. The jumps in p, ρ and T across the shock can be evaluated from (71). They are strongly amplified by global gas compression as the piston moves towards the cylinder endwall.

In the present case as well as more general cases that will be considered in §5.4, the piston motion and the internal dissipation of the shock both contribute to variations in shock amplitudes. The contribution from the piston is positive if it does work on the wave field; negative when acoustic energy is extracted by the piston. The effect of shock dissipation is always negative. In view of the significant shock attenuation caused by its internal dissipation, as illustrated in the first fundamental solution, the latter mechanism should not be ignored when interpreting results involving a moving piston.

5.4. *Solutions with arbitrary piston motion*

The nonlinear amplitude equation (64) can be rewritten as

$$\frac{\mathrm{d}}{\mathrm{d}\tau}\left(\frac{1}{A}\right) = -\tfrac{1}{4}(\gamma+1)\rho_0\left(\frac{\bar{U}_p}{A}-1\right). \tag{76}$$

When integration is carried out by using (34) and (65), the result is obtained in a remarkably simple form:

$$\frac{1}{A} = \rho_0^{-\frac{1}{4}(\gamma+1)}\left[\frac{1}{A_i}+\tfrac{1}{4}(\gamma+1)\int_0^{\tau}\rho_0^{\frac{1}{4}(\gamma+5)}(\hat{\tau})\,\mathrm{d}\hat{\tau}\right]. \tag{77}$$

Equation (77) shows that $A(\tau)$ is indeed positive-definite for any $A_i > 0$. The integral in (77) is believed to be associated with the accumulated internal dissipation of the shock, because its monotone growth with time always contributes negatively to the shock amplitude. It is in fact the term that causes the shock to decay in (74), (75), where $\rho_0 = 1$. In general, the shock amplitude depends on the global density ρ_0, and thus the shock dissipation is also a function of ρ_0. The effects of piston-generated compression and expansion are included in ρ_0, which is related to piston velocity through (35), (36). One observes from (77) that the initial wave amplitude A_i has little influence on the long-time solution of A, which always approaches zero.

If A_i is negative, the right-hand side of (77) must vanish at a certain time instant as the integral grows. This leads to unbounded shock amplitudes, and is clearly unacceptable. As mentioned earlier, physically this branch of solutions corresponds to spurious rarefaction shocks that violate the second law of thermodynamics.

In order to study quantitatively the effect of piston acceleration on $A(\tau)$, (77) is evaluated numerically for the case of a constantly accelerating piston, $\bar{U}_p = 1 + a\tau$.

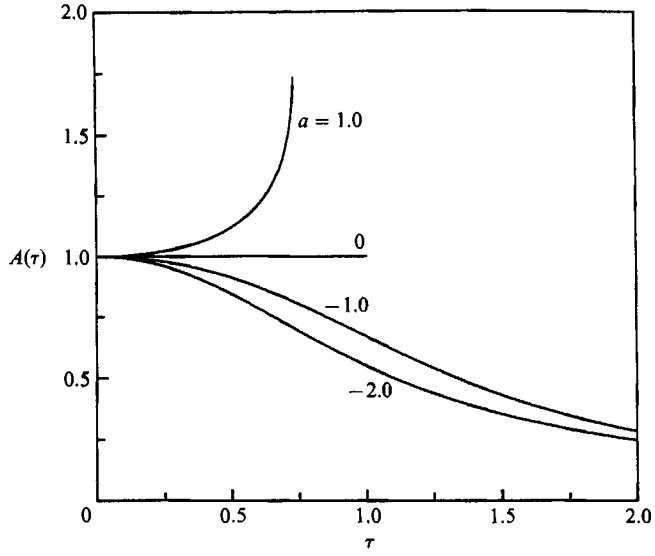

FIGURE 8. Time variation of velocity jump $A(\tau)$ across the shock wave generated by impulsive piston motion, $\bar{U}_p = 1 + a\tau$, as calculated from (77).

The sudden start of the piston at $\tau = 0$ generates a shock of $A_i = 1$ in the originally quiescent gas. Results are shown in figure 8 for four selected values of piston acceleration. If the piston acceleration a is positive, as is the case of $a = 1.0$ shown by the upmost curve in figure 8, the velocity jump A increases monotonically with τ. Since the difference between $\bar{U}_p$ and $A(\tau)$ provides the driving potential for the latter (cf. (64)), the value of A may never exceed $\bar{U}_p$. The piston reaches the opposite cylinder wall when $\tau = \sqrt{3} - 1$, beyond which the solution for A is physically meaningless and is ignored. The horizontal straight line in figure 8 corresponds to the second fundamental solution mentioned previously, for a constant-speed piston motion ($a = 0$), in which case the driving potential is zero, and $A(\tau)$ remains constant always. The piston reaches the cylinder endwall when $\tau = 1$. On the other hand, if a is negative, the velocity jump associated with the shock is seen to decrease with τ, as is seen from figure 8 for the cases of $a = -1$ and -2. In these two cases, the deceleration process reverses the direction of the piston motion before it ever reaches the cylinder endwall. As the piston accelerates further in the negative direction, A approaches zero asymptotically.

Given the jump value of velocity across the shock, the corresponding jumps for pressure and other thermodynamic properties can be evaluated from (71). It is important to note that although the normalized jump values of u, p, ρ and T are proportional to one another (cf. (72), (73)), their absolute values do not behave in the same manner, owing to the ρ_0-dependent coefficients in (71). For example, if the cylinder gas undergoes a compression process by a decelerating piston, as are the cases of $a = -1$ and $a = -2$ before the piston reaches the uppermost points, then according to the above analysis $A(\tau)$ decreases with time, while the value of ρ_0 increases. The combined effect of A and ρ_0 may cause both magnification and damping in the jump values of p, ρ and T, depending on the relative magnitudes of the two effects.

The pressure variations at the piston face are shown in figures 9(*a*) and 9(*b*), for the cases $a = 1$ and $a = -1$ respectively. The variations in bulk pressure are also

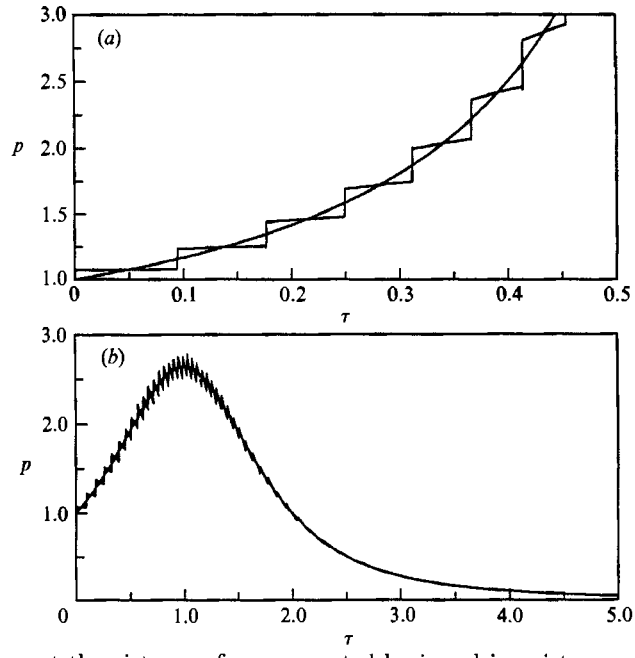

FIGURE 9. Pressure at the piston surface, generated by impulsive piston motion, $\bar{U}_p = 1 + a\tau$, into an initially static gas. The initial piston Mach number $\epsilon = 0.05$. Case (*a*) $a = 1$, case (*b*) $a = -1$.

shown as the centred, smooth lines. When $a = 1$ both A and ρ_0 increase monotonically with time. Thus the pressure jump upon each shock reflection on the piston surface, as shown in figure 9(*a*), also increases with time. The frequency of shock passage increases as the forward-moving piston compresses the cylinder gas. Between two successive shock reflections the gas pressure rises smoothly as an accumulative effect of passages of continuous compression signals generated at the piston face. As the piston acceleration continues the stronger compression signals cause faster pressure rise, thus increasing the slopes of the continuous p–τ curve sections. When $a = -1$ (cf. figure 9*b*) the bulk gas pressure rises at first as the piston travels forward with decreasing velocity, until it becomes zero. Subsequently the piston starts to move backward, producing an expansion process in the gas. From figure 9(*b*) it is seen that during the compression stage the pressure jump increases with increasing mean pressure, even though the velocity jump is monotonically decreasing. During the expansion process both velocity and pressure jumps decrease. The variations in shock passage frequency and the slopes of the continuous p–τ curve sections can be explained by using the same reasoning as employed for figure 9(*a*).

It is worth pointing out that although the results in figures 8 and 9 are obtained for constant piston acceleration, they are characteristic of a more general class of piston motion. An analysis of (64) shows that as long as $\bar{U}_p$ is a monotonic function of τ, $\mathrm{d}A/\mathrm{d}\bar{U}_p$ is always positive. The amplitude $A(\tau)$ approaches either $\bar{U}_p$ or zero, depending on the sign of $\bar{U}_p$.

If, on the other hand, $\bar{U}_p'(\tau)$ changes sign during the piston motion, the variations of $A(\tau)$ and $\bar{U}_p(\tau)$ are not always in phase. In the physical system both compression and expansion signals coexist, resulting in a more complex response of the velocity jump across the shock. As an example of this case the periodic piston motion used in the study by Klein & Peters (1988),

$$\bar{U}_p(\tau) = \tfrac{1}{2}\pi \cos(\pi\tau), \tag{78}$$

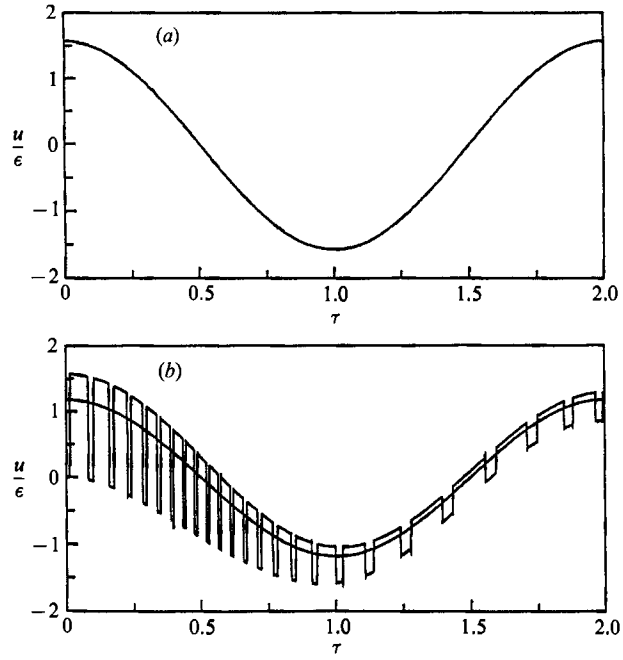

FIGURE 10. Velocity variations at specified material points s, generated by impulsively started, periodic piston motion, $\bar{U}_p = \frac{1}{2}\pi \cos(\pi\tau)$, in an initially static gas. The characteristic piston Mach number $\epsilon = 0.05$. Case (*a*) $s = 0$, case (*b*) $s = \frac{1}{4}$.

is employed. The shock is again induced by the impulsive piston motion at $\tau = 0$, so that $u_i = 0$. Plotted in figures 10(*a*) and 10(*b*) are velocity variations of the gas particles at $s = 0$ and $s = \frac{1}{4}$ respectively, for a complete cycle of piston motion. The corresponding pressure variations are depicted in figures 11(*a*) and 11(*b*). As in the previous figures, the smooth lines in figures 10 and 11 represent the bulk response of the gas. The jumps in both velocity and pressure correspond to shock passage at the given mass location. The material point at $s = \frac{1}{4}$ experiences twice as many shock passages as does the piston face, because it receives the shock from both directions. The two neighbouring time intervals between successive shock passages in figures 10(*b*) and 11(*b*) are not equal, owing to the different shock round-trip times between the mass point at $s = \frac{1}{4}$ and the two confining solid walls. It is important to notice from figures 10 and 11 that there is damping of the shock after one cycle of piston motion. Calculations for longer time duration show that the shock wave will further decay away after repeated cycles of the piston stroke, as is illustrated in figure 12, where both $A(\tau)$ and $\bar{U}_p$ are depicted *vs.* τ. $A(\tau)$ decreases with τ in an oscillatory manner. The local maxima and minima of A are reached whenever $A = \bar{U}_p$, as is expected from (64). On the same figure, the velocity jump of a shock propagating in a static piston–cylinder system, as calculated from (74), is also depicted as the dashed line. Since the latter purely represents the effect of shock-generated dissipation, it appears that the overall damping of the shock during the cyclic piston motion is due to its internal dissipation. The piston produces localized amplification and damping to the shock during different phases of its oscillation.

The results in figure 11(*a*) for $0 \leqslant \tau \leqslant 1$ are in agreement with figure 6 in Klein & Peters' (1988) study, based on a qualitative comparison of the respective pressure

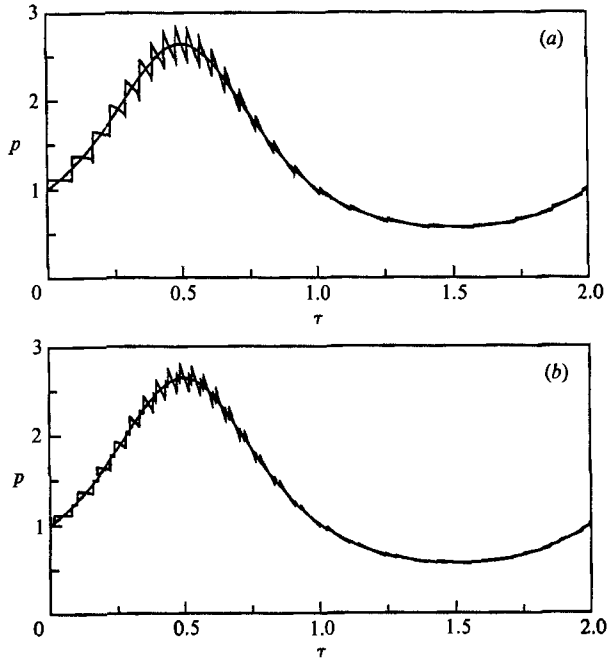

FIGURE 11. Pressure variations at specified material points s, generated by impulsively started, periodic piston motion, $\bar{U}_p = \frac{1}{2}\pi \cos(\pi\tau)$, in an initially static gas. The characteristic piston Mach number $\epsilon = 0.05$. Case (*a*) $s = 0$, case (*b*) $s = \frac{1}{4}$.

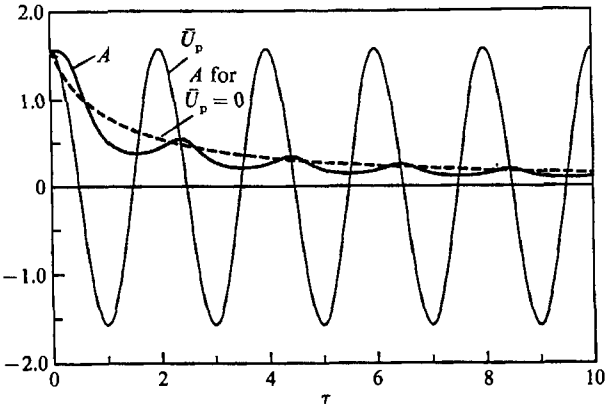

FIGURE 12. Time variation of velocity jump $A(\tau)$ across the shock generated by impulsively started, periodic piston motion $\bar{U}_p = \frac{1}{2}\pi \cos(\pi\tau)$, as calculated from (77). The dashed line is the value of $A(\tau)$ for a shock of identical initial amplitude, when the piston remains static, as calculated from (74).

curves. A similar result has been reported by Schneider (1981). In both of the earlier studies only pressure variations on the piston surface for the first half-cycle of the piston motion were shown, and the damping of the shock was attributed solely to the expansion signals emitted from the piston.

Finally, this section is concluded by emphasizing that the transformation (60) allows physically meaningful solutions to the infinite system (43) only for $A_1 \geqslant 0$. Under this circumstance the solution developed above provides the unique weak solution to the Euler equations. If $A_1 < 0$, however, Euler equations have an infinite

number of mathematically weak solutions. Since the transformation (60) does not allow the rarefaction discontinuity to be flattened out, the solution obtained represents a propagating rarefaction shock which is physically irrelevant. In this case one has to solve the approximate version of the infinite system (43), (44) instead, in order to obtain physically meaningful solutions. One example has already been demonstrated in §4.3, for the case of an impulsively started piston motion with a negative constant velocity.

6. Concluding remarks

In the present study an analytical procedure is combined with numerical techniques to analyse the evolution of small-amplitude waves in a variable-volume cylinder. The solutions are written as eigenfunction expansions with spatially harmonic basis functions (cf. (49) and (50)). The time-dependent Fourier coefficients consist of products of fast-varying harmonic functions and more slowly varying functions. The latter are computed from a system of the coupled, nonlinear ordinary differential equations (43) and (44). This method is seen to be equivalent to the spectral method, which has found wide use in recent years in solving certain types of partial differential equations. The numerical results obtained in this study suggest that the method can be used most effectively to provide approximate solutions to hyperbolic systems in the absence of spatial and temporal discontinuities.

The truncation errors associated with the presence of shocks in the evaluation of (43) and (44) deserve special attention because they destabilize the solution. To assess the effect of the truncation errors on the discontinuous solutions, the density variations on the piston surface in the case of an impulsively started, constant-velocity piston motion, are evaluated based on both the truncated version of (43), (44) and (50), and the exact solution (67) where $A = 1$. The results are illustrated in figures 13(*a*) and 13(*b*) respectively where 200 Fourier terms are summed. Obviously, the truncation error appears first as a small cusp on the solution curve in figure 13(*a*), which is magnified gradually as it propagates at the local sound speed. Apart from the cusped regions the solution is not appreciably affected by the truncation error. It is the same as the correct solution shown in figure 13(*b*). This is typical for all the example calculations which involve shock formation conducted in our study. Since the truncation errors do not spread out randomly in the solution, one can easily detect the first sign of error in the solution. Before it occurs the solution is reliable. It is important to observe that the erroneous signal always originates after the shock formation, and once it is formed, it follows the shock wave with a phase lag of π.

The similarity transformation (60) allows great simplifications and much improved accuracy for a class of solutions that contain a travelling shock embedded between two straight lines of identical slope in a confined domain, or sawtooth solutions. These solutions describe the long-time limiting shapes for shocks formed from a smooth compression wavefront, as discussed in §4, as well as shocks generated by impulsively started piston motion. The nonlinear response of shock amplitude to the piston motion is described by (77).

In comparison to the more conventionally employed method of characteristics, the Fourier series technique is seen to possess the following advantages in solving the present gasdynamic problem: (i) The solution procedure is simple and straightforward. Since there is no need for transformations of independent variables, it is not necessary to expand the time and space variables in the asymptotic procedures. (ii) The resulting secular equations are ordinary rather than partial differential

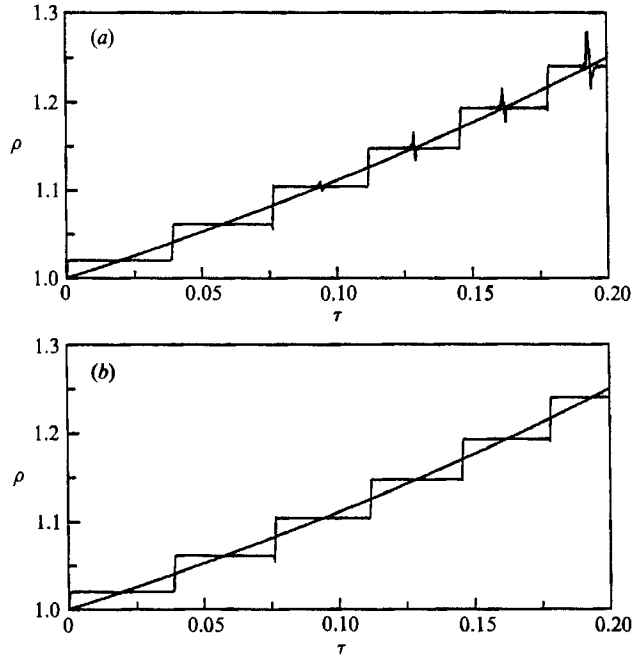

FIGURE 13. Density variations of the gas on the piston surface, due to impulsively started piston motion $\bar{U}_p = 1$. The piston Mach number $\epsilon = 0.02$. (*a*) Based on the truncated version of (43), (44) and (50); (*b*) based on solution (67) where $A = 1$.

equations. This allows solutions by a relatively simple numerical technique. (iii) Physical interpretation of the results is straightforward. One can readily identify from the analytical expressions the bulk effects and the acoustic phenomena, and the interactions between them. (iv) Special treatment associated with shock waves, necessary when the characteristics method is used, can be avoided. The shock location as well as the Rankine–Hugoniot jump conditions are obtained naturally from the series solutions.

The description of shock waves by the method of characteristics inevitably leads to spurious multivalued regions. The area rule (Whitham 1974) provides a universally valid remedy to help select the physically meaningful solutions. The Fourier series description of a shock is simpler in this respect because it is necessarily single-valued. On the contrary, for waves generated by rarefaction discontinuities, such as the case of an impulsively started backward piston motion, the method of characteristics always provides the unique correct solution, while the Fourier series solutions of the Euler equations are not unique. In this case solutions based on the similarity transformation technique (cf. (60) and (77)) and the truncated version of (43) and (44) are both mathematically acceptable. There is, however, also a remedy to the uncertainty based on the well-known entropy theory (Lax 1973). The solution based on (60) and (77) must be dismissed as it describes a spurious expansion shock, while the other solution, exemplified in figure 5, is the physically relevant solution.

The major drawback of the current method lies in its inaccuracy in describing the wave field after the shock formation but before it reaches the sawtooth asymptotic state, due to large truncation errors in approximating the infinite equation system (43) and (44). One possible approach to overcome this difficulty is to divide the physical region into two parts of variable length, separated by the travelling shock

discontinuity. Fourier series representations may be employed to construct solutions on either side of the shock, while Rankine–Hugoniot conditions may be applied to relate the two continuous solutions across the shock. In that case better convergence of the Fourier series can be expected because they are only used to represent continuous solutions. The feasibility of this proposal is currently under investigation.

The following conclusions can be drawn from the mathematical analysis of the present study: In a gas-filled piston–cylinder system, small-amplitude gasdynamic waves can be generated by initial disturbances in velocity as well as thermodynamic state of the gas. The waves, whose amplitudes are of comparable magnitudes with the small piston Mach number ϵ, are nonlinear in nature on the timescale of piston motion. As they propagate back and forth repeatedly inside the cylinder, nonlinear effects cause deformation of the waveform. Weak shock formation will occur from an initially continuous compression wavefront. Repeated passage of the gasdynamic waves generate the accumulative effect of bulk gas response to the piston motion, which are to order ϵ identical to those from equilibrium thermodynamic calculations. This bulk variation of the background-gas state does not alter the nonlinear wave deformation and shock formation processes in a fundamental way. The shock formation time increases with decreasing amplitude of the disturbance. The frequency of wave passage in the cylinder increases as the gas is compressed and decreases when it expands. Long-time shock evolution as well as impulsively started piston compression result in a sawtooth-like wave field. The shock strength depends on the piston velocity and the bulk density of the gas. The internal dissipation causes significant attenuation of the shock.

This work was supported by grants from the Mathematical Science Program of the Army Research Office DAAG29-85-K-0209 and DAAL03-88-K-0111. The authors wish to thank Professor Nobert Peters and Dr Rupert Klein of RWTH, Aachen, West Germany, and Professor Patrick D. Weidman of the University of Colorado for their helpful comments and enlightening suggestions during the development of this work. The erudite comments of an anonymous referee were helpful in relating the present work to earlier studies that were previously unknown to the authors.

REFERENCES

BETCHOV, R. 1958 Nonlinear oscillations of a column of gas. *Phys. Fluids* **1**, 205–212.

CHESTER, W. 1964 Resonant oscillations in closed tubes. *J. Fluid Mech.* **18**, 44–64.

CHU, B. T. 1963 Analysis of a self-sustained nonlinear vibration in a pipe containing a heater. *Phys. Fluids* **6**, 1638–1644.

GEAR, C. W. 1971 *Numerical Initial Value Problems in Ordinary Differential Equations.* Prentice-Hall.

HINDMARSH, A. C. 1974 GEAR: Ordinary Differential Equation Solver. *Lawrence Livermore Laboratory, Rep.* UCID-30001 (Revision 3).

KASSOY, D. R. 1979 The response of a confined gas to a thermal disturbance: Slow transients. *SIAM J. Appl. Maths* **36**, 624–634.

KLEIN, R. & PETERS, N. 1988 Cumulative effects of weak pressure waves during the induction period of a thermal explosion in a closed cylinder. *J. Fluid Mech.* **187**, 197–230.

KLUWICK, A. 1981 The analytical method of characteristics. *Prog. Aerospace Sci.* **19**, 197–313.

KUFNER, A. & KADLEC, J. 1971 *Fourier Series.* London: Iliffe Books.

LANDAU, L. D. & LIFSHITZ, E. M. 1959 *Fluid Mechanics.* Pergamon.

LAX, P. D. 1973 *Hyperbolic Systems of Conservation Laws and the Mathematical Theory of Shock Waves.* SIAM Regional Conference Series in Applied Mathematics, Vol. 11.

LIGHTHILL, M. J. 1949 A technique for rendering approximate solutions to physical problems uniformly valid. *Phil. Mag.* **40**, 1179–1201.

LIGHTHILL, M. J. 1978 *Waves in Fluids.* Cambridge University Press.

LIN, C. C. 1954 On a perturbation theory based on the method of characteristics. *J. Maths Phys.* **33**, 117–134.

MORSE, P. M. & INGARD, U. I. 1968 *Theoretical Acoustics.* McGraw-Hill.

OCHMANN, M. 1985 Nonlinear resonant oscillations in a closed tube – An application to the averaging method. *J. Acoust. Soc. Am.* **77**, 61–66.

RADHWAN, A. M. & KASSOY, D. R. 1984 The response of a confined gas to a thermal disturbance: II Rapid boundary heating. *J. Engng Maths* **18**, 133–156.

ROTT, N. 1980 Thermoacoustics. *Adv. Appl. Mech.* **20**, 135–174.

SCHNEIDER, G. H. 1981 Kompression und Expansion eines Gases in einem Zylinder als Störproblem. *Acta Mech.* **41**, 157–184.

SMOLLER, J. 1983 *Shock Waves and Reaction-Diffusion Equations.* Springer.

TEMKIN, S. 1969 Propagating and standing sawtooth waves. *J. Acoust. Soc. Am.* **45**, 224–227.

WANG, M. 1989 Piston generated dynamic compression and expansion of an inert gas in a cylinder. Ph.D thesis, University of Colorado, Boulder.

WANG, M. & KASSOY, D. R. 1990*a* Dynamic compression and weak shock formation in an inert gas due to fast piston acceleration. *J. Fluid Mech.* **220**, 267–292.

WANG, M. & KASSOY, D. R. 1990*b* Dynamic response of an inert gas to slow piston acceleration. *J. Acoust. Soc. Am.* **87**, 1466–1471.

WHITHAM, G. B. 1974 *Linear and Nonlinear Waves.* John Wiley and Sons.